Monte-Carlo Simulation of

Stellar Intensity Interferometry

by

Janvida Rou

A Senior Honors Thesis Submitted to the Faculty of

The University of Utah

In Partial Fulfillment of the Requirements for the

Honors Degree of Bachelor of Science

In

The Department of Physics and Astronomy

Approved:

Stephan LeBohec Supervisor	David Kieda Chair, Department of Physics
Anil Seth Department Honors Advisor	Sylvia D. Torti Dean, Honors College

May 2012

Abstract

Stellar intensity interferometers will allow for achieving stellar imaging with a tenth of a milli-arcsecond resolution in the optical band by taking advantage of the large light collecting area and broad range of inter-telescope distances offered by future gamma-ray Air Cherenkov Telescope (ACT) arrays. Up to now, studies characterizing the capabilities of ACTs used as intensity interferometers have not accounted for certain realistic effects that will be encountered when collecting actual data. In this paper, we present the semi-classical quantum optics Monte-Carlo simulation we developed in order to investigate these experimental limitations. Using this tool we present our first results using our simulation model to investigate sensitivity and imaging capability limitations associated with telescopes spatial extension, photodetectors and electronics pulse shape, and excess noise.

Contents

1. Introduction and general principles

1.1. Intensity Interferometry. Stellar Intensity Interferometry (SII) is an experimental method for measuring the angular diameter of optical sources and acquiring high resolution images of stars. In a stellar intensity interferometer the light from a star is received by two or more detectors separated by a baseline that may range from tens of meters to kilometers which allows for resolution of surface features ranging from less than $0.1\,mas$ (longest baseline) to $10\,mas$ (shortest baseline) at visible wavelengths. Intensity interferometry relies on the correlation between the light intensity fluctuations recorded by different telescopes (Brown and Twiss, 1957). The fluctuations contain two components: the wave noise and the shot noise. The dominant component is the shot noise which is the inherent random fluctuation associated with the photon statistics, and which is uncorrelated between telescopes. The smaller component is the wave noise which can be interpreted as the beating between different Fourier components of the light incident on the telescopes. The wave noise shows correlation between different telescopes provided there is some degree of mutual coherence in the light.

The light intensity correlation between receivers is measured as the time-integrated product of the fluctuations δi_1 & δi_2 in the photodetector currents. Although higher order correlations can be of interest (Fontana (1983); Gamo (1963); Sato et al. (1978); Jain and Ralston (2008); Ofir and Ribak (2006a); Ofir and Ribak (2006b)), throughout this paper we restrict ourselves to two-point correlations. In the case of a thermal light source and an ideal system, the two point correlation is equal to the squared

degree of coherence $|\gamma|^2$ of the light at the two telescopes:

$$|\gamma|^2 = \frac{\langle \delta i_1 \delta i_2 \rangle}{\langle i_1 \rangle \langle i_2 \rangle} \tag{1}$$

where $\langle \cdots \rangle$ represents a time average. According to the van Cittert-Zernike Theorem (Zernike, 1938), the complex degree of coherence, γ, is the normalized Fourier transform of the intensity distribution of the source. One difficulty associated with image reconstruction using SII is that the measurable quantity is the squared degree of coherence $|\gamma|^2$ which means that information about the phase of the Fourier transform is lost. Methods of phase recovery and image reconstruction employ algorithms such as the Cauchy-Riemman approach, Gerchberg-Saxton phase retrieval, or generalized expectation maximization. These techniques recover the phase lost from squaring the Fourier transform. For further details see Nuñez et al. (2012). It has been shown that when these methods are applied with a sufficient number density of different baselines between telescopes, images of stars can be reconstructed with a relatively high degree of accuracy (Nuñez et al., 2010). For example, SII can provide stellar imaging to investigate various topics of interest including stellar rotation, limb darkening (Nuñez et al., 2012), mass loss in Be-stars, surface temperatures inhomogeneities (Dravins et al., 2010), and binary systems.

Unlike amplitude (Michelson) interferometry, which depends on the phase differences in the light waves received at the detectors, SII depends on the phase difference between the low frequency beats which are accessible with the instrumentation signal bandwidth. Hence, SII only requires control of the path of the light to an accuracy set by the electronic bandwidth (Note: A system with a $1\,GHz$ signal bandwidth does

not suffer from path length differences of up to a few centimeters). As a consequence, SII presents advantages: it is essentially insensitive to atmospheric turbulence, it does not require high quality optics, and it permits large baseline and short wavelength measurements without extra difficulties. However, since SII relies on a second order effect, it is a less sensitive technique which requires larger light collectors and longer integration times when compared with amplitude interferometry. Nevertheless, as optical quality requirements are much less stringent than for amplitude interferometry, these light collectors can be constructed at a relatively low cost.

It was shown by Robert Hanbury Brown and Richard Twiss that the signal to noise ratio (SNR) for an intensity correlation measurement with an ideal system can be written as (Hanbury Brown, 1974)

$$SNR = A\,\alpha\,n\,|\gamma|^2\sqrt{\Delta f\,T/2} \tag{2}$$

where A is the effective light collecting area of the telescopes, α is the quantum efficiency of the photodetectors, n ($photon \cdot m^{-2} \cdot s^{-1} \cdot Hz^{-1}$) is the spectral density of the light, Δf is the signal bandwidth of the photodetectors and electronics, and T is the total time of integration (Hanbury Brown, 1974). It is worth noting that the SNR is independent of the optical bandwidth used for the observations. This expression for the SNR only accounts for the photon statistics, previously referred to as the shot noise. The factor of $\sqrt{2}$ accounts for the fact that starlight is nonpolarized. If we consider fully polarized light then the signal-to-noise ratio is increased by a factor of

$\sqrt{2}$. In recent publications discussing the potentials of reviving SII, the van Cittert-Zernike Theorem was used together with the above SNR expression to estimate the performances and capabilities of SII arrays.

1.2. Narrabri Stellar Intensity Interferometer. Intensity interferometry was developed in the early 1950s by R. Hanbury Brown as a technique for measuring the angular diameters of radio sources. Later, it was applied to stars in the optical range. In the 1960s Hanbury Brown successfully used this technique with the Narrabri Stellar Intensity Interferometer (NSII) in order to measure the angular diameter of 32 stars (Hanbury Brown et al., 1974). The NSII was in operation from 1963 to 1974 and consisted of two $6.5\,m$ telescopes which were movable along a system of circular tracks. The mobility of the telescopes on a circular track allowed the telescopes to track any star while always keeping the baseline between the telescopes perpendicular to the direction to the star. In addition, the signals were correlated in a control building located at the center of the track, which eliminated the need to introduce time delays to bring the two signals in time.

The correlator used by the NSII was a four transistor based linear multiplier. Because the instantaneous signal is inherently significantly smaller than the random fluctuations resulting from Poisson statistics, the signal was resolved by integration over many ($\sim$100 s) time intervals. Effects of the overall signal offsets and drifts were filtered out by applying phase switching at different frequencies to both channels. Since Hanbury Brown made his measurements with the NSII, intensity interferometry has been abandoned in favor of Michelson interferometry as a method for imaging stars (Labeyrie et al., 2006), (Lawson et al., 1999).

1.3. Toward a modern stellar intensity interferometer array. There has been a recent increase of interest in SII because of the advantages it may offer in terms of cost and compatibility with existing or future Very High Energy (VHE) gamma-ray Air Cherenkov Telescope (ACT) arrays (Weekes, 2003), which operate by taking advantage of the Cherenkov light flashes that atmospheric showers produce. Because the atmospheric Cherenkov light is very faint, observations of VHE gamma-rays require large light collectors and are restricted to low moonlight nights. During moonlit nights, ACT arrays cannot be used for gamma-ray observations, but they could be used for SII observations through narrow optical bandwidths. The implication is that SII measurements could be performed with ACT arrays without interfering much with the VHE observation programs.

In preparation for large scale projects like the Cherenkov Telescope Array (CTA) (Actis et al., 2010) there are several ongoing efforts to experimentally investigate the feasibility and potential of SII, one of which is at the StarBase Observatory in Grantsville, Utah (LeBohec et al., 2010). StarBase consists of two $3\,m$ telescopes separated by a baseline of $23\,m$. The electronics implemented at StarBase are more modern than what was available at the time of the NSII and they offer the benefit of better signal processing technology. With an array of two telescopes we would be able to demonstrate the potential of SII and identify the best approaches by measuring the angular diameter of bright stars or by resolving a bright binary star system such as Spica.

Arrays such as CTA could consist of up to ∼100 telescopes providing thousands of different baselines simultaneously and offering detailed imaging capabilities. In previous studies characterizing imaging capabilities and sensitivity, it has been assumed that the detectors are pointlike in size so the van Cittert-Zernike Theorem applies directly and the degree of correlation between the intensity fluctuations recorded by different telescope is strictly the squared magnitude of the Fourier transform of the source radiance. In reality, when the size of the telescope apertures becomes comparable to the baseline required to resolve features of interest on a source, then the light is no longer fully coherent across individual apertures (Hanbury Brown, 1974). This results in correlation data that departs from a pure Fourier transform.

Additionally other instrumentation-related systematic effects were neglected in previous studies. For example, electronic artifacts such as noise, single photon pulse shapes, excess noise, and inaccuracies in the adjustment of the delay lines or tracking all affect the signal or contribute to the degradation of the SNR. Also, the effect of the night sky background contamination integrated in the point spread function (PSF) of the light collector and the profile of the optical band pass has only been qualitatively or very approximatively taken into account. Furthermore, high speed digitization electronic systems are considered to be used for SII applications as they offer the flexibility of offline signal correlation analysis. The development of data analysis algorithms require realistic simulated data. All of these aspects are important for the performance characterization and data analysis preparation for the design and deployment of an SII observatory. In this paper we present a Monte-Carlo simulation of a semi-classical quantum description of light and an instrumentation model we

developed in order to investigate these and other realistic instrumentation-related limitations. In section 2 we describe our simulation approach which we validate through applications to ideal cases, and then we include a first model of instrumentation imperfections. In section 3 we present a few applications characterizing instrumentation related effects concentrating on the finite telescope size, the single photon pulse shape, and the excess noise. Finally in section 4, we summarize our findings.

2. Photon level Monte-Carlo simulation of SII

2.1. Thermal light source and telescope signals. Following the description provided by, we model a stellar light source with photon flux Φ ($photon \cdot m^{-2} \cdot s^{-1}$) within a given optical bandwidth as a discrete collection of M point sources of equal flux $\Phi_M = \frac{\Phi}{M}$. Each point source is then defined by a wave amplitude $\mathcal{A}_j$, an angular frequency ω_j, a phase ϕ_j, and an angular position $\theta_j = (\theta_x, \theta_y)$. At a given time the phase ϕ_j of the light is taken randomly and uniformly from $[0, 2\pi]$ and the amplitude $\mathcal{A}_j$ is taken randomly from a Gauss deviate (Mandel and Wolf, 1995) of mean zero and variance $\overline{\mathcal{A}_j} = \sqrt{\frac{\Phi_M}{c}}$, where c is the speed of light. In order to make the simulation closer to the continuous distribution of a realistic stellar source, at each time step we also randomly set the angular frequency ω_j and angular position $\theta_j = (\theta_x, \theta_y)$ of each point source from distributions corresponding to the spectral density spectrum and radiance of the simulated stellar source.

Then, we model each extended telescope as a set of small light collecting elements of area dA_k centered on position $X_k = (x_k, y_k)$. Note that "small" in this context means that each light collecting element is small enough that it cannot individually resolve features of the light source, or more strictly, that the mutual degree of coherence between any two points of an area element is maximal.

The average number of photons incident on one area element k of the telescope during a time δt can be written:

$$\overline{d\mu_k} = dA_k \cdot \delta t \cdot c \left| \sum_j \mathcal{A}_j e^{i\left(\omega_j (\frac{\theta_j \cdot X_k}{c}) + \phi_j\right)} \right|^2 \tag{3}$$

Where throughout this paper, we use $\langle \cdots \rangle$ to denote a time average and $\overline{\cdots}$ to denote a statistical average.

The average number of photons collected by a telescope i during a given timestep can then be written:

$$\bar{\mu}_i = \sum_k \overline{d\mu_k} \tag{4}$$

Then the actual number of photons reaching telescope i in a time δt is given by $n_i = P(\bar{\mu}_i)$ where $P(m)$ represents a Poisson deviate of mean and variance m. The summation of the waves prior to taking the magnitude is responsible for the non-purely Poisson light intensity fluctuations, previously referred to as wave noise, displaying correlation between the different telescopes.

For a source with photon flux Φ, the average number of photons emitted by the light source and incident on the telescope in a time δt is $\bar{n}_i = \Phi \cdot A_i \cdot \delta t$ where A_i is the total light collecting area of telescope i. If for the time being we ignore the signal bandwidth limitation and we consider the instantaneous telescope signal output s_i to be AC coupled then we can write $s_i = n_i - \bar{n}_i$, where we use $\bar{n}_i = \langle \bar{\mu}_i \rangle$ so as to ensure $\langle s_i \rangle = 0$.

2.2. Realistic signal simulation. With the description provided thus far, we can in principle simulate any intensity interferometry signal, taking the timestep to be smaller than the coherence time τ_c of the light. However, in reality, the electronic time resolution, or signal bandwidth, is much greater than the coherence time so it is desirable to be able to produce these simulations with timesteps $\delta t \gg \tau_c$ so as to make the computation time manageable.

To do this, we artificially dilute the correlated photons from our earlier calculation with a stream of purely Poisson-distributed photons. Contaminating the star light with purely Poisson light degrades the signal-to-noise ratio as would degrading the signal bandwidth, permitting simulations with $\delta t \gg \tau_c$. As we have seen in section 2.1, the average number of photons collected by a telescope in a time interval δt is $\bar{n} = \Phi \cdot A \cdot \delta t$. With $\bar{\mu}_i$ calculated as described above, the number of photons incident on the telescope in a time interval δt is a random variable of unknown statistics with mean $\bar{n}$. Recalling that $\langle \mu \rangle = \bar{n}$, we model the signal from telescope i in terms of a number of photons per time-step as

$$s_i = P(\bar{n}(1-\alpha) + \bar{\mu}_i \alpha) - \bar{n} \tag{5}$$

where $P(m)$ represents a Poisson deviate. We have introduced the parameter α, which sets the degree of dilution of the correlated photons without affecting the total photon rate. We see that $\alpha = 0$ corresponds to a case in which the correlation is zero, while $\alpha = 1$ corresponds to a case of maximal correlation. The signal s_i, which is realistically AC coupled, is artificially constructed here in such a way that $\bar{s}_i = 0$ by subtracting the mean number of photons in each time step. The correlation is computed as $c_{12} = \frac{\langle s_1 \cdot s_2 \rangle}{\bar{n}_1 \cdot \bar{n}_2}$. We have found that $c_{12} = \alpha^2 |\gamma|^2$ (see Appendix 5.1) in the limit that the diameter of the telescopes is small compared to the distance required to begin to resolve surface features of the star, and we numerically find that $\alpha = \sqrt{\frac{\tau_c}{\delta t}}$. Note that α is equivalent to the $\sqrt{\Delta f \, T}$ term in Eq. 2 with $\Delta f = \frac{1}{\delta t}$. In these single measurements, the instantaneous signal-to-noise ratio can be calculated only per coherence time, so we correct by a factor of τ_c intstead of T.

2.3. Photodetector and electronic pulse model. Ideally, each incident photon would be represented by a Dirac peak that occurs exactly at the time when the photon is detected. To more realistically model the signal of an SII measurement, we must consider the fact that photons are measured by electronic systems with a specific time response. We model an AC coupled signal as a pulse that has a positive component for short amount of time (a few ns) and which is constructed using with a double exponential with an integral normalized to one. The AC coupling is obtained by adding to the main pulse a negative tail which is the result of the convolution product of the pulse with an exponential of unit integral and characteristic time, set to the actual AC coupling time constant.

We expect that the sensitivity of our system degrades as the square root of the signal bandwidth Δf (see Eq. 2) and hence the square root of the inverse of the width of the main pulse. With the detailed pulse model, see Figure 1, we may evaluate the sensitivity more precisely and investiage the effects of experimental timing inaccuracies.

Detector excess noise consists of noise produced by the photomultiplier tube (PMT). It is determined primarily by the fluctuations in the number of electrons emitted at the first dynode of the PMT. This results in fluctuations in the amplitude of the single photon response pulse. We model the excess noise by multiplying the amplitude of each single photon response pulse by a random variable of Gauss distribution centered on the most likely response amplitude and truncated to eliminate negative amplitude responses. As a consequence, the mean is greater than the

most probable amplitude. In order for the mean single photon response amplitude to remain the same, all signals are divided by the mean of the excess noise distribution.

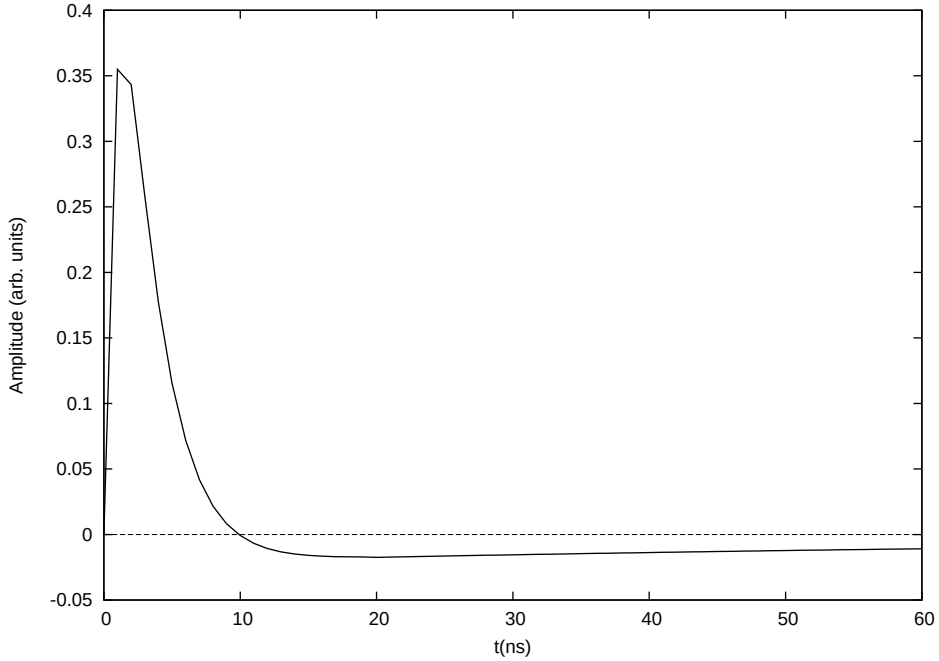

FIGURE 1. Pulse shape used to model real electronic signals. The main pulse is followed by an AC coupled negative tail whose integral is artifically constructed in such a way that the integral of the pulse is zero.

2.4. Proof of principle of the light model. To test that our simulations yield the correct correlation, we simulated a uniform disk star and calculated c_{12} as a function of the baseline. The results, shown in Figure 2, are compared with the profile of an Airy disk which is the squared modulus of a perfect Fourier transform of a uniform disk. We found that the fewer the number of point sources which we consider to make up the star, the greater the power at high frequencies, which causes $|\gamma|^2$ to deviate from the Airy disk. Additionally, we find that randomizing the location of each point source within the spatial extension of the star as well as randomizing the

frequency emitted by each point source at each time step further reduces deviations from the Airy disk, as shown in Figure 3.

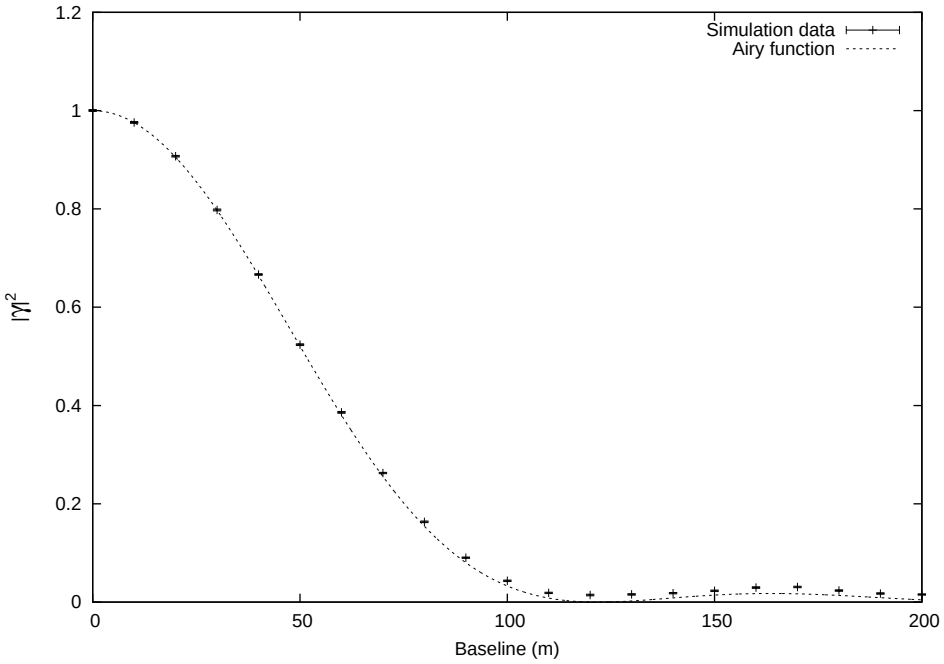

FIGURE 2. Simulated data for a pointlike telescope reproduces an airy function

To further test our simulation, we compared the expected SNR calculated from Eq. 2 to the standard deviation of simulated correlations. We run each numerical experiment 50 times in order to calculate the standard deviation of each set of experimental parameters. We varied the pulse width (signal bandwidth) and flux, see Figure 4 for the results. For the signal bandwidth, a square pulse was used so that the width of the pulse is unambiguous. The AC coupling was taken into account by subtracting the average signal rather than including a negative tail for the pulse, so the correlation is obtained between signals s_i as described in section 2.1. We varied the width of the pulse from $1\,ns$ to $30\,ns$ and verified that the standard deviation evolved as a square root of the pulse width. Similarly, we tested the flux of the light source from $1 \cdot 10^8\ photons \cdot m^{-2} \cdot s^{-1}$ to $1 \cdot 10^9\ photons \cdot m^{-2} \cdot s^{-1}$, which approaches

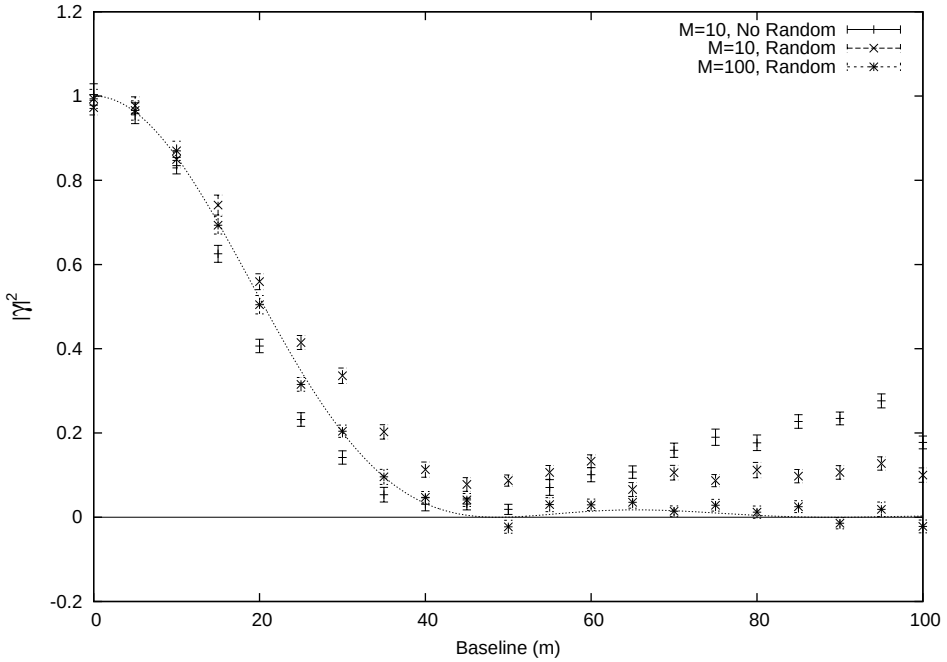

FIGURE 3. Simulated data. Deviations at large baselines are greatest when the star is simulated with a fewer number of points and when the points of the star are not randomized at each timestep.

the limit in which our calculations hold. We verified that the SNR evolved with the inverse of the flux as expected from Eq. 2. The effect on the SNR of varying the flux is equivalent to varying the light collecting area of the detectors. The effects of increasing the size of the aperture will be further discussed in Section 3.1. These results confirm that our Monte-Carlo model provides correct results in simple cases, and so we can begin to investigate more subtle instrumentation artifacts.

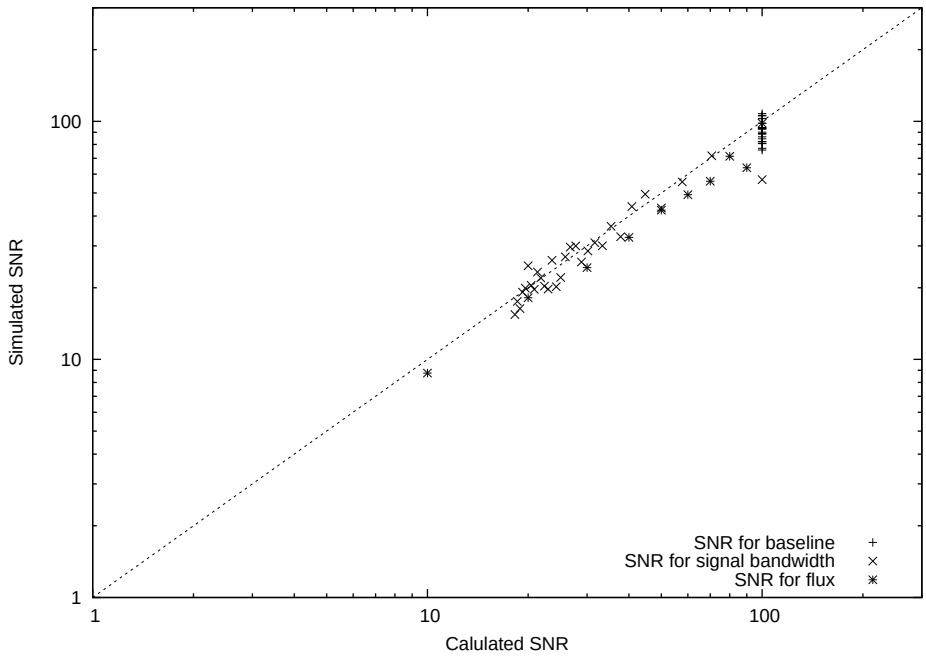

FIGURE 4. Statistics of simulation results are shown to follow the theoretical signal to noise prediction by Hanbury Brown. The ratio of the simulated to expected signal to noise ratio for various parameters fall around a 1:1 ratio.

3. Application of realistic simulations

3.1. Mirror extension. The results of the extended mirror simulation are shown in Figure 5 for various telecope diameters which are comparable to the dish sizes considered by CTA (Actis et al., 2010). We see that the shape of the ideal curve, which is shown by the Airy disk profile and by the simulated data for the case of a pointlike detector, is smoothed out as the size of individual detectors increases and begins to resolve the star. In principle the effect of large detector sizes on the degree of correlation is equivalent to taking a double convolution of $|\gamma|^2$ with the effective light collecting area of the telescope (see Appendix 5.2) (Hanbury Brown, 1974), which moves $|\gamma|^2$ away from being the squared magnitude of the Fourier transform of the source. We verify this by taking the double convolution of the simulated data for a

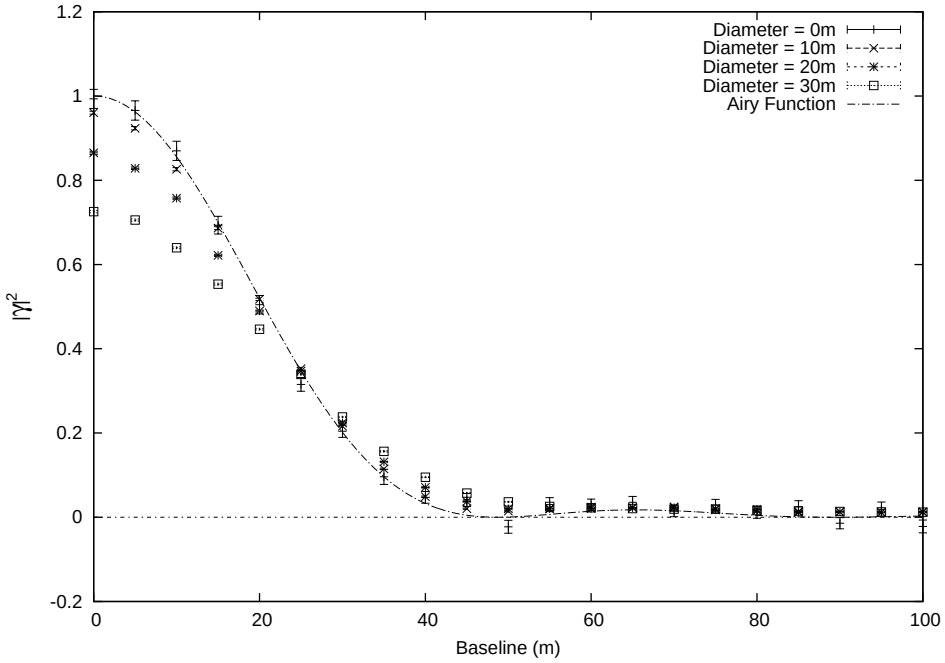

FIGURE 5. $|\gamma|^2$ plotted against baseline for various telescope dish sizes.

pointlike telescope with a uniform disk of some diameter and checking that it matches with the simulated data for a telescope of the same diameter. This is shown in Figure 6 for the case of a $20\,m$ telescope.

When the effect of the telescope extension is important, corrections must be applied to the data before the van Cittert-Zernike Theorem can be used. Simulations can be exploited to establish this correction. The mirror extension effects are significant, and corrections must be applied in most cases, since telescopes that may be constructed in future arrays such as CTA could be up to $\sim 30\,m$ in diameter (Actis et al., 2010), which is sufficiently large to begin resolving some stellar features.

3.2. Excess noise. We find that the signal-to-noise ratio has a linear dependence on the detector excess noise present in the system as shown in Figure 7. The effect is small and must be averaged over a large number of experiments to be evident. Figure

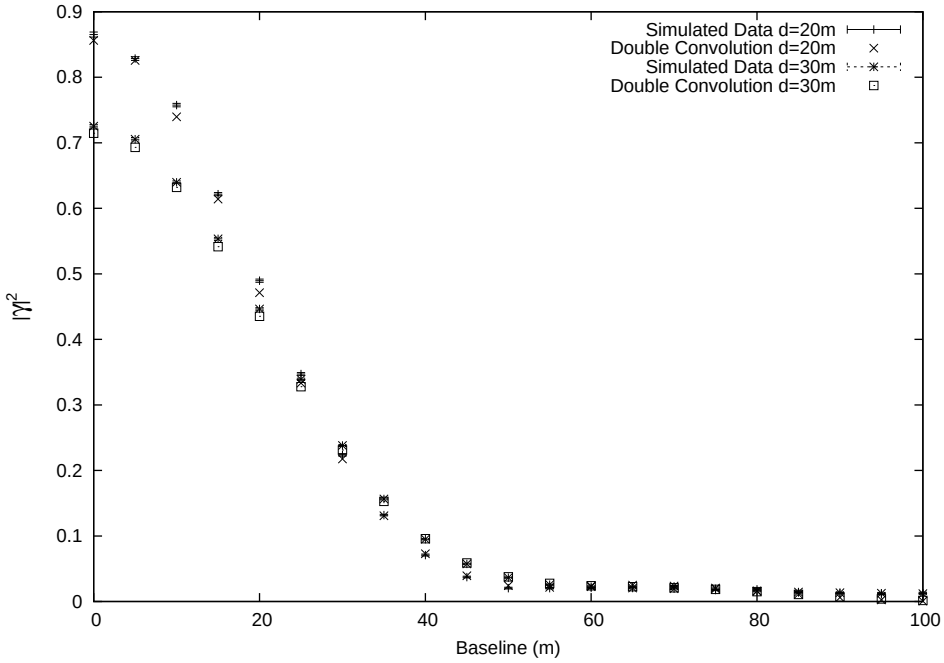

FIGURE 6. Double convolution of simulated data (d=0) with a uniform disk (d=20).

7 also shows our current model, which is still under construction, for the excess noise. We see that our preliminary model deviates from the simulation most significantly for larger values of the excess noise. This is due to the truncation that we apply to avoid producing negative single photon response pulse amplitudes.

3.3. Further applications. Our simulation may be used to study numerous additional effects regarding realistic SII measurements. For example, delays must be used to bring the signals in time to the different telescopes. The simulations can be used to investiage the effects of inaccuracies in the time alignment of the signals. Furthermore, ACT optics are generally Davies-Cotton designed (Davies and Cotton, 1957), which is not isochronous. In previous studies, this was approimatively accounted for as a signal bandwidth limitation. With our simulation we can now simulate isochronous effects in detail.

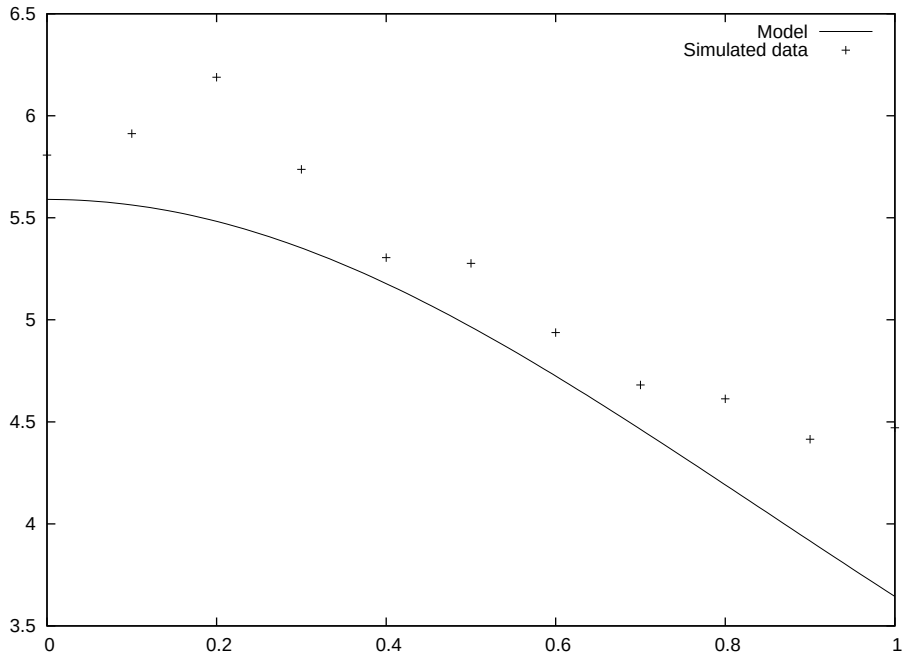

FIGURE 7. Dependence of signal-to-noise ratio on excess noise and current model of excess noise

Also for example, we could investigate the effect of stray light contamination. When very faint stars are to be observed, the observation time must be long enough in order to obtain a sufficient signal-to-noise ratio for the measurement. In these cases, contamination from the night sky background, especially during bright moonlit nights, cannot be ignored. When the light received is dominated by the night sky background contamination, increasing the observation time is no longer beneficial. Consequently, stray light contamination ultimately limits the faintness of stars that can be observed. These limitations can be investigated with our simulation for each specific observation. Stray light is included in the simulation as a stream of aditional phontons with purely Poisson statistics. The simulation allows to introduce any level of stray light contamination and predict its effect on the measurement sensitivity.

A possible technological approach to SII consists in digitizing the individual telescope signal. The required fast digitization rate (greater than $100\,Ms/s$) implies huge volumes of data must be handled. However, this provides a lot of flexibility as the correlation is obtained off-line at the time of data analysis. Our simulations combined with a model of the digitizer can be used to develop and optimize the analysis.

In addition to using the simulations to study realistic effects, we may also study artificial physical situations which may be of applicational or technological interest. For example, the simulation may be used to study non-thermal sources which would not encounter from looking at stars, but which may nevertheless be encountered in some situations. For a non-thermal source, such as an ideal astrophysical laser, in the extreme case, the distributions of the electric fields may have deviations of Gaussianity. In the extreme case of a laser, we would expect to see no change in the correlation as a function of the baseline, however, we would expect to see the correlation change as a function of time delay in one channel.

4. Conclusion

Previous studies have not accounted for many realistic effects associated with SII measurements. Here we have demonstrated that our simulation correctly reproduces the expected behavior associated with SII and we have briefly discussed problems such as telecope mirror extension, excess noise, time delay, signal bandwidth limitation, stray light contamination, and signal digitization. We have found that the result of a spatially extended detector is a double convolution of the ideal case with a uniform disk identical to the detector area. We also verified that the signal-to-noise ratio has a small but noticable linear dependence on the excess noise present in the system.

With our simulation, we are able to observe these effects which would allow us to correct for them in experimental efforts. In addition, we are able to simulate any SII measurement and specify optimal conditions and parameters necessary to measure any given system.

In addition to simulating general effects for realistic systems, we also would be able to simulate real measurements. In the future, SII measurements at StarBase may be attempted on sources such as the binary star system, Spica. If such measurements are successful, we may use our simulation to verify and support experimental data.

5. Appendix

5.1. Partially correlated Poisson Statistics. A photon stream of modulated mean μ (i.e. $\langle\mu\rangle = n$) can be diluted by a stream of photons of purely Poisson statistics while maintining the average photon rate by writing:

$$s_i = P(\bar{n}(1-\alpha)) + P(\mu\alpha) - \bar{n} = P(\bar{n}\tilde{\alpha}) + P(\mu\alpha) - \bar{n} \tag{6}$$

where we have introduced $\tilde{\alpha} = 1 - \alpha$.

It is a property of Poisson statistics that

$$\text{if } x_i = P(m_i) \textit{ then } \sum x_i = P(\sum m_i)$$

The converse of this property is Raikov's theorem which states that if the sum of two random independent variables is Poisson distrubted, then so is each of the two random independent variables.

We are interested in the correlation between the fluctuations between the two signals $c_{12} = \frac{\langle s_1 \cdot s_2 \rangle}{\bar{n}^2}$. We consider

$$\langle s_1 \cdot s_2 \rangle = \langle (P_1(\bar{n}\tilde{\alpha}) + P_1(\mu_1\alpha) - \bar{n})\,(P_2(\bar{n}\tilde{\alpha}) + P_2(\mu_2\alpha) - \bar{n}) \rangle \tag{7}$$

where P_1 and P_2 are Poisson deviates for the number of photons in the different telescopes 1 and 2. Developing:

$$\begin{aligned}
\langle s_1 \cdot s_2 \rangle \;=\; & \langle P_1(\bar{n}\tilde{\alpha}) P_2(\bar{n}\tilde{\alpha}) \rangle + \langle P_1(\bar{n}\tilde{\alpha}) P_2(\mu_2\alpha) \rangle + \langle P_2(\bar{n}\tilde{\alpha}) P_1(\mu_1\alpha) \rangle \\
& - \bar{n}\langle P_1(\bar{n}\tilde{\alpha}) + P_2(\bar{n}\tilde{\alpha}) \rangle - \bar{n}\langle P_1(\mu_1\alpha) + P_2(\mu_2\alpha) \rangle \\
& + \langle P_1(\mu_1\alpha) P_2(\mu_2\alpha) \rangle + \bar{n}^2
\end{aligned}$$

Developing each term, we find that

$$\langle s_1 \cdot s_2 \rangle = \alpha^2 \langle (\mu_1 - \bar{n}) \cdot (\mu_2 - \bar{n}) \rangle \tag{8}$$

Identifying $\langle (\mu_1 - \bar{n}) \cdot (\mu_2 - \bar{n}) \rangle$ as the degree of correlation between the non-diluted signals, and hence equal to $|\gamma|^2$ implies that $c_{12} = \alpha^2 |\gamma|^2$. So it appears that diluting the original signals by a factor $\frac{1}{\alpha}$ scales the degree of correlation by a factor α^2 for which we need to apply a correction.

5.2. Effect of detector area on the complex degree of coherence. We choose to set the origin of the coordinate system at the light source. Points on the source are labeled by positions $\vec{x}'$ with respect to the origin. The same points labeled with respect to a far away observer at position $\vec{x}$ are dentoed:

$$\vec{r} = \vec{x} - \vec{x}'. \tag{9}$$

For a point-like detector, the observed electric field at $\vec{x}$ is

$$E(\vec{x}, t) = \int \frac{A(\vec{x}', t)}{|\vec{r}|} e^{i(kr - \omega t + \phi(\vec{r}, t))} d^2x', \tag{10}$$

Where $\phi(\vec{r}, t)$ is a random phase caused by atmospheric turbulence among other factors. Now we make the approximation

$$|\vec{r}| \approx |\vec{x}| - \vec{x}' \cdot \frac{\vec{x}}{|\vec{x}|}, \tag{11}$$

so that

$$E(\vec{x},t) = \frac{e^{ikx}}{|\vec{x}|}\int A(\vec{x}',t)\, exp\left\{i\left(k\vec{x}'\cdot\frac{\vec{x}}{|\vec{x}|} - \omega t + \phi(\vec{r},t)\right)\right\} d^2x'. \tag{12}$$

If the detector has a finite area, then the electric field at position $\vec{x}$ is a superposition of electric fields detected at positions $\vec{x} - \vec{x}_d$, where $\vec{x}_d$ are points in the detector with respect to position $\vec{x}$. The random phase can be expressed as a function of detector coordinates as $\phi(\vec{x}_d, t)$. Now the superposition of electric fields is expressed as a convolution with the detector area, i.e.

$$E(\vec{x},t) \approx \frac{e^{ikx}}{|\vec{x}|}\int A(\vec{x}',t)\, exp\left\{i\left(k\vec{x}'\cdot\frac{\vec{x}-\vec{x}_d}{|\vec{x}|} - \omega t + \phi(\vec{x}_d,t)\right)\right\} d^2x' d^2x_d. \tag{13}$$

To calculate the time averaged correlation between detectors i and j, denoted as $\langle E(\vec{x}_i)E^*(\vec{x}_j)\rangle$, we should note that

$$\left\langle A(\vec{x}',t)A(\vec{x}'',t)e^{i(\phi(\vec{x}_{di},t)-\phi(\vec{x}_{dj},t))}\right\rangle = I(\vec{x}')\delta(\vec{x}'-\vec{x}'')\delta(\vec{x}_{di}-\vec{x}_{dj}), \tag{14}$$

where $I(\vec{x}')$ is the light intensity at point $\vec{x}'$. This is because separate points on the source are not correlated over large distances. The phase is also not correlated between separate points, that is, $\phi(\vec{x}_{di},t) - \phi(\vec{x}_{dj},t)$ will only be zero when $x_{di} = x_{dj}$; otherwise it will have a time variation which results in $\left\langle e^{i(\phi(\vec{x}_{di},t)-\phi(\vec{x}_{dj},t))}\right\rangle = 0$ when $x_{di} \neq x_{dj}$.

Now defining $\vec{z}_i \equiv \vec{x}_i - \vec{x}_{di}$, the time averaged correlation is

$$\langle E(\vec{x}_i)E^*(\vec{x}_j)\rangle = C\int I(\vec{x}')\, exp\left\{ik\left(\vec{x}'\cdot\frac{\vec{z}_i}{|\vec{x}_i|} - \vec{x}'\cdot\frac{\vec{z}_j}{|\vec{x}_j|}\right)\right\} d^2x' d^2x_{dj}. \tag{15}$$

where C is a constant. When $|\vec{x}'| \ll |\vec{x}_j|$, we can write the angle $\vec{\theta}$ as

$$\vec{\theta} \equiv \frac{\vec{x}'}{|\vec{z}_j|}, \tag{16}$$

We can now express the correlation as

$$\langle E(\vec{x}_i)E^*(\vec{x}_j)\rangle = \int I(\vec{\theta})\, e^{-ik\vec{\theta}\cdot(\vec{z}_i-\vec{z}_j)}\, d^2\theta\, d^2x_{dj} \tag{17}$$

$$= \int \tilde{I}(\vec{z}_i - \vec{z}_j)\, d^2x_{dj}, \tag{18}$$

where $\tilde{I}(\vec{z}_i - \vec{z}_j)$ is the Fourier transform of the radiance distribution of the star, which goes from angular space to detector separation space. Now the quantity measured in intensity interferometry is

$$|\gamma(\vec{x_i}, \vec{x_j})|^2 = \frac{|\langle E(\vec{x}_i)E^*(\vec{x}_j)\rangle|^2}{\sqrt{|E(\vec{x}_i)|^2|E(\vec{x}_j)|^2}} \tag{19}$$

$$= \frac{1}{I(\vec{x}_i)I(\vec{x}_j)} \int |\tilde{I}(\vec{z}_i - \vec{z}_j)|^2\, d^2x_{di} d^2x_{dj}. \tag{20}$$

Therefore, we see that the effect of having finite sized telescopes is to replace the magnitude of mutual degree of coherence $|\gamma|^2$ by its double convolution with the telescope light collection area shape.

Bibliography

M. Actis, G. Agnetta, F. Aharonian, and et al. Design Concepts for the Cherenkov Telescope Array. 2010.

Robert Hanbury Brown and Richard Q. Twiss. Interferometry of the intensity fluctuations in light. i. basic theory: The correlation between photons in coherent beams of radiation. *Proceedings of the Royal Society of London. Series A. Mathematical and Physical Sciences*, 242(1230):300–324, 1957.

John M. Davies and Eugene S. Cotton. Design of the quartermaster solar furnace. *Solar Energy*, 1:16 – 22, 1957.

Dainis Dravins, Hannes Jensen, Stephan LeBohec, and Paul Nunez. Stellar Intensity Interferometry: Astrophysical targets for sub-milliarcsecond imaging. *Proc.SPIE Int.Soc.Opt.Eng.*, 7734:77340A, 2010.

Peter R. Fontana. Multidetector intensity interferometers. *Journal of Applied Physics*, 54(2):473 –480, 1983.

Hideya Gamo. Triple correlator of photoelectric fluctuations as a spectroscopic tool. *Journal of Applied Physics*, 34(4):875–876, 1963.

Robert Hanbury Brown. *The intensity interferometer*. Halsted Press, 1974.

Robert Hanbury Brown, J Davies, and L.R. Allen. The angular diameters of 32 stars. *Monthly Notices of the Royal Astronomical Society*, 167(1):121–136, 1974.

Pankaj Jain and John Ralston. Direct determination of astronomical distances and proper motions by interferometric parallax. *A&A*, 484(3):887–895, 2008.

Antoine Labeyrie, Stephen Lipson, and Peter Nisenson. *An introduction to optical stellar interferometry*. Cambridge University Press, 2006.

P. R. Lawson, T. R. Scott, and C. A. Haniff. Group-delay tracking and visibility fluctuations in long-baseline stellar interferometry. *Monthly Notices of the Royal Astronomical Society*, 304(1):218–224, 1999.

Stephan LeBohec, Ben Adams, Isobel Bond, Stella Bradbury, Dainis Dravins, et al. Stellar intensity interferometry: Experimental steps toward long-baseline observations. *Proc.SPIE Int.Soc.Opt.Eng.*, 7734:773448, 2010.

Leonard Mandel and Emil Wolf. *Optical coherence and quantum optics*. Cambridge University Press, 1995.

Paul Nuñez, Stephan LeBohec, David Kieda, Richard Holmes, Hannes Jensen, and Dainis Dravins. Stellar intensity interferometry: imaging capabilities of air Cherenkov telescope arrays. In *Society of Photo-Optical Instrumentation Engineers (SPIE) Conference Series*, volume 7734, 2010.

Paul Nuñez, Richard Holmes, David Kieda, and Stephan LeBohec. High angular resolution imaging with stellar intensity interferometry using air cherenkov telescope arrays. *Monthly Notices of the Royal Astronomical Society*, 419(1):172–183, 2012.

Paul Nuñez, Richard Holmes, Dave Kieda, Janvida Rou, and Stephan LeBohec. Imaging sub-milliarcsecond stellar features with intensity interferometry using air Cherenkov telescope arrays. *Monthly Notices of the Royal Astronomical Society*, 2012.

Aviv Ofir and Erez N. Ribak. Offline, multidetector intensity interferometers i. theory. *Monthly Notices of the Royal Astronomical Society*, 368(4):1646–1651, 2006a.

Aviv Ofir and Erez N. Ribak. Offline, multidetector intensity interferometers ii. implications and applications. *Monthly Notices of the Royal Astronomical Society*, 368(4):1652–1656, 2006b.

Takuso Sato, Shusou Wadaka, Jiro Yamamoto, and Junichi Ishii. Imaging system using an intensity triple correlator. *Applied Optics*, 17(13):2047–2052, 1978.

Trevor Weekes. *Very high energy gamma-ray astronomy*. Taylor and Francis, 2003.

Frits Zernike. The concept of degree of coherence and its application to optical problems. *Physica*, 5(8):785 – 795, 1938.

Name of Candidate:	Janvida Rou
Birth Date:	April 14, 1990
Birth Place:	Salt Lake City, Utah
Address:	115 South 1400 East Salt Lake City, UT, 84112